Synthesis, Microstructural Characterisation and Magnetic Study of Two New One-Dimensional Members of the $(A_3ZnMnO_6)_\alpha$ $(A_3Mn_3O_9)_\beta$ Homologous Series (A = Ba, Sr)

María Hernando,*[a] Khalid Boulahya,[a] Marina Parras,[a] and José M. González-Calbet[a]

Keywords: Electron diffraction / Electron microscopy / One-dimensional oxides / Magnetic properties / Twinned microstructure

Two new members of the $(A_3ZnMnO_6)_\alpha(A_3Mn_3O_9)_\beta$ one-dimensional homologous series have been synthesised with the compositions $Sr_4Mn_2ZnO_9$ and $Ba_5Mn_3ZnO_{12}$. Their structures can be described as a hexagonal array of infinite 1D-chain polyhedra, running parallel to the *c*-axis, formed by two face-sharing octahedra linked by one trigonal prism for $Sr_4Mn_2ZnO_9$, and one more octahedron between prisms for $Ba_5Mn_3ZnO_{12}$. Both oxides have a twinned microstructure as evidenced by SAED and HREM. $Sr_4Mn_2ZnO_9$ shows a pronounced antiferromagnetic character with a broad susceptibility maximum at 100 K due to short-range ordering. At low temperature, the susceptibility data suggest a transition to a 3D long-range ordering.

Introduction

The family of one-dimensional oxides structurally related to the 2H hexagonal perovskite ABO_3 [1] has been widely studied due to their striking magnetic properties. This structure and the K_4CdCl_6 [2] structural type define the two end-members of this 1D family. Both structures are formed by a hexagonal array of infinite chains of face-sharing polyhedra running parallel to the *c*-axis. In the 2H hexagonal type, $[BO_6]$ octahedra (O_h) constitute the polyhedra chains, whereas in K_4CdCl_6 ($A_3A'BO_6$) one $[BO_6]$ octahedron alternates with one $[A'O_6]$ trigonal prism (TP) in an ordered sequence. Between both structures, an unlimited number of one-dimensional related structures can be generated by varying the octahedron/trigonal-prism ratio.[3−6] There are several ways to describe the different members of this family. Among them, a very useful approach is to consider these structures as being formed by the ordered intergrowth of the structural units building up the two end-members. This building principle gives rise to the $(A_3A'BO_6)_\alpha(A_3B_3O_9)_\beta$ general formula, where α and β denote the number of $A_3A'BO_6$ and 2H-ABO_3 structural blocks, respectively, in each member.[7] A large number of oxides belonging to this family have already been reported. Usually, the A cation is an alkaline earth metal whereas the chemical nature of A′ and B is much wider since alkali, alkaline earth, transition, rare earth or main group metals can occupy such positions.

A wide range of magnetic properties are observed in these oxides. When both trigonal prism and octahedral sites contain magnetic cations, the system presents a 1D magnetic behaviour that can induce a 3D ordered state at low temperature.[8−10] However, this 1D character can be lost — a 3D character appearing — when diamagnetic cations separate the paramagnetic ones in the chain.[9,11] In this case, the superexchange pathways between such paramagnetic cations are not significantly shorter than those between metals located at different chains, hence the intrachain and interchain interactions are of comparable magnitude.

Up to now, only two phases have been stabilised in the A−Mn−Zn system (A = Ca and Ba), *viz.* Ca_3MnZnO_6 [9] and $Ba_6Mn_4ZnO_{15}$.[12] The former adopts the K_4CdCl_6 structure corresponding to the (α = 3 β = 0) member of the $(A_3A'BO_6)_\alpha(A_3B_3O_9)_\beta$ homologous series. The structure can be regarded as infinite 1D-chains, running along the *c*-axis, made up of alternate $[ZnO_6]$ face-sharing trigonal prisms and $[MnO_6]$ octahedra (Figure 1a). The magnetic cations are only located in the octahedral holes and, consequently, the $(Mn\text{-}Mn)_{intrachain}$ distances (5.3 Å) are similar to the $(Mn\text{-}Mn)_{interchain}$ distances (5.6 Å), giving rise to a 3D magnetic system.

$Ba_6Mn_4ZnO_{15}$,[12] which is isostructural to $Sr_6Co_5O_{15}$,[13] shows a different magnetic behaviour. This 1D-oxide corresponds to the (α = 3 β = 3) member of the above-mentioned homologous series. The chains are now made up of four face-sharing octahedra linked by one trigonal prism (Figure 1d). The cationic distribution in the different polyhedra is only partially ordered. Zn and Mn occupy the trigonal prismatic site in equal concentrations, with the re-

[a] Departamento de Química Inorgánica, Facultad de Químicas, Universidad Complutense
28040 Madrid, Spain
E-mail: jgcalbet@quim.ucm.es

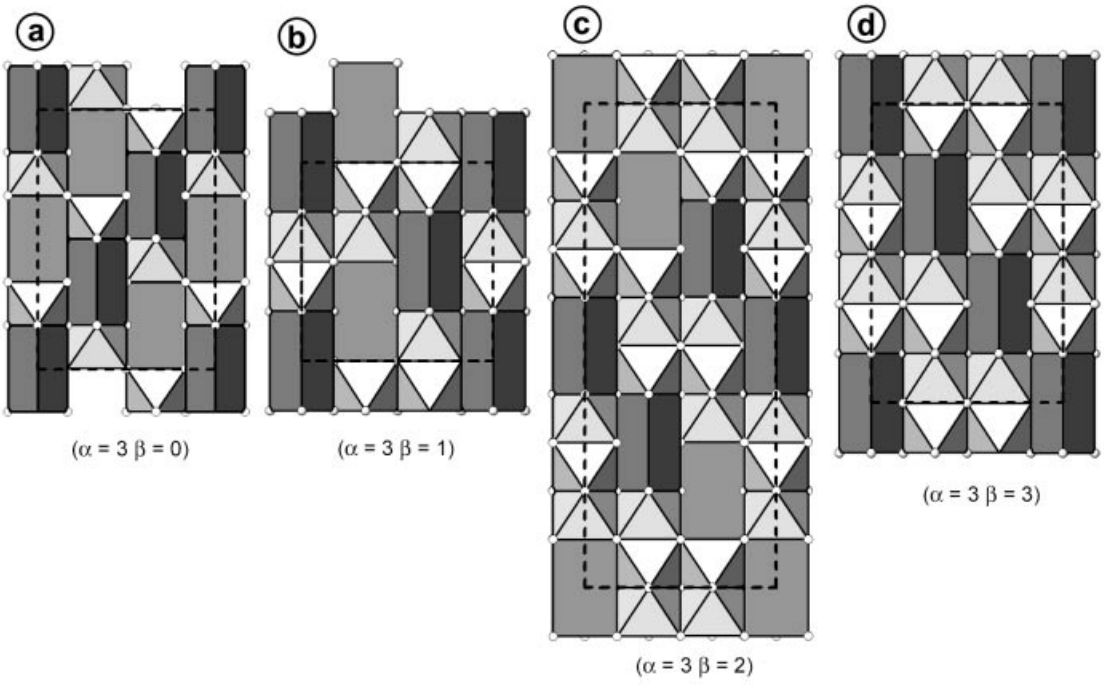

Figure 1. Schematic structures of Ca_3MnZnO_6 (a) and $Ba_6Mn_4ZnO_{15}$ (d), the ($\alpha = 3\,\beta = 0$) and ($\alpha = 3\,\beta = 3$) members of the $(A_3ZnMnO_6)_\alpha(A_3Mn_3O_9)_\beta$ homologous series; ideal structures correspond to intermediate phases of this series: the ($\alpha = 3\,\beta = 1$) (b) and the ($\alpha = 3\,\beta = 2$) (c) members; the unit cells are indicated by dotted lines

maining Zn and Mn distributed in the octahedral sites. A 1D magnetic ordering along the chains is observed due to antiferromagnetic interactions between Mn^{IV} ions. However, the presence of nonmagnetic Zn^{2+} cations in the octahedral environment suppresses the intrachain interaction between Mn atoms and, consequently, magnetic trimers, dimers and isolated $[Mn^{IV}O_6]$ octahedra are created. Uncompensated magnetic moments of the trimers and the isolated octahedra are responsible for the rise in the magnetic susceptibility at low temperature.

Between Ca_3MnZnO_6 ($\alpha = 3\,\beta = 0$) and $Ba_6Mn_4ZnO_{15}$ ($\alpha = 3\,\beta = 3$), two intermediate members can be envisaged. Actually, Figure 1b and 1c correspond to the ideal structures of the ($\alpha = 3\,\beta = 1$) and ($\alpha = 3\,\beta = 2$) terms of the above family. Therefore, in order to synthesise these novel 1D phases containing Mn as the only magnetic cation, we have explored the A−Mn−Zn−O system (A = Ba, Sr,) which has resulted in the stabilisation of $Sr_4Mn_2ZnO_9$ ($\alpha = 3\,\beta = 1$) as a single phase. Attempts to isolate the ($\alpha = 3\,\beta = 2$) term have been successful for the $Ba_5Mn_3ZnO_{12}$ composition although some impurities have been detected. Structurally, both phases can be regarded as a hexagonal array of infinite 1D-chains of face-sharing polyhedra running parallel to the crystallographic *c*-axis. In $Sr_4Mn_2ZnO_9$, two octahedra are linked by one trigonal prism, whereas in $Ba_5Mn_3ZnO_{12}$ one more octahedron is incorporated between the trigonal prisms in the polyhedra rows. The synthetic conditions, microstructural characterisation and magnetic properties are discussed.

Results and Discussion

Figure 2a shows the powder XRD pattern corresponding to $Sr_4Mn_2ZnO_9$. The whole pattern can be indexed on the basis of a trigonal unit cell (*P*321) with parameters $a = 0.9592(1)$ and $c = 0.7823(1)$ nm. On the other hand, the XRD pattern corresponding to $Ba_5Mn_3ZnO_{12}$ (Figure 2b), can be also indexed in a trigonal ($P\bar{3}c1$) unit cell with $a = 1.0060(1)$ and $c = 2.0812(1)$ nm. In fact, both patterns show the characteristic profile of one-dimensional oxides corresponding to the $(A_3A'BO_6)_\alpha(A_3B_3O_9)_\beta$ homologous series,[7] although some broad reflections are observed.

The SAED study sheds more light on the microstructural features of both compounds. For this purpose, it is helpful to consider these one-dimensional oxides as commensurate modulated superstructures of the 2H-hexagonal type. As we have previously reported, the superstructure direction can be expressed as $[\alpha+\beta\ \alpha+\beta\ i\ 2\alpha]^*_{2H}$ [7] and, thus, is related to the number of α and β blocks constituting every phase. The superstructure direction is determined from the $[1\bar{2}10]$ zone axis, which provides the most useful structural information.

$Sr_4Mn_2ZnO_9$

Figure 3a corresponds to the above-mentioned $[1\bar{2}10]$ zone axis of the $Sr_4Mn_2ZnO_9$ sample. All the observed crystals show the same features. The most intense spots correspond to hexagonal 2H planes (referred as sub-index 2H in the figure). The modulation direction, marked with an ar-

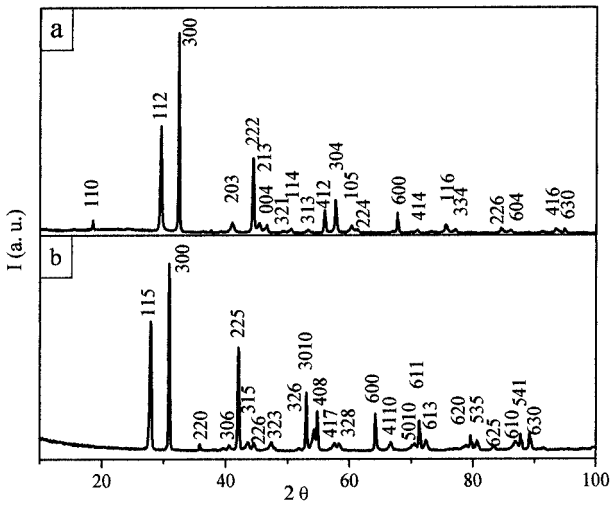

Figure 2. Powder XRD patterns of $Sr_4Mn_2ZnO_9$ (a) and $Ba_5Mn_3ZnO_{12}$ (b)

row, follows the reciprocal $[44\bar{8}6]^*_{2H}$ direction, according to the ($\alpha = 3$ $\beta = 1$) values. However, the features of this SAED pattern also indicate that the microstructure of this 1D-phase must be more complex than that shown by other isostructural oxides. Actually, if this reciprocal plane is compared to the same reciprocal net corresponding to the $(Sr_{0.5}Ca_{0.5})_4Co_3O_9$ isostructural oxide[14] (Figure 3b), some differences can be appreciated. Both SAED patterns present the same structural characteristics but the intensity distribution of the superstructure spots is clearly different. The modulated intensity of such spots, as observed in $(Sr_{0.5}Ca_{0.5})_4Co_3O_9$, is typical of this structure. Following the $[44\bar{8}6]^*_{2H}$ direction, the first-order satellite reflections are the most prominent ones, the intensity decreasing as the satellite order increases. On the contrary, in $Sr_4Mn_2ZnO_9$, such a modulation is not only noticeable along the $[44\bar{8}6]^*_{2H}$ direction but also at 90°, i.e., following the $[\bar{4}\bar{4}86]^*_{2H}$ direction. This feature could be due to twinning, as previously observed in isostructural $Sr_4CuIr_2O_9$.[15]

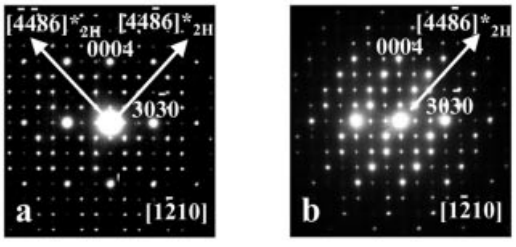

Figure 3. SAED patterns along the $[1\bar{2}10]$ zone axis of $Sr_4Mn_2ZnO_9$ (a) and $(Sr_{0.5}Ca_{0.5})_4Co_3O_9$ (b)

The multitwinned microstructure was confirmed by HREM. The image taken along the $[1\bar{2}10]$ zone axis is shown in Figure 4a. Several domains, tilted 90° to one another around the *c*-axis, are clearly evident. In each domain, d-spacings of 0.83 and 0.78 nm along the *a* and *c* axes, respectively, are observed and these correspond to d_{100} and d_{001} of the ($\alpha = 3$ $\beta = 1$) one-dimensional oxide. The contrast variation in each domain is also characteristic of this member of the series. This is clearly seen in the magnification of one of them (Figure 4b), where it can be observed that, following the *c*-axis, one bright dot alternates with two less-intense ones. We have previously reported that, in all these 1D oxides, the metal columns in the trigonal interstices and the Sr atoms are imaged as bright dots.[16] Therefore, the contrast sequence in this experimental image is as expected for the ...O_hO_hTP... polyhedral sequence in the 1D-chains. The calculated image (inset of Figure 4b) shows a good fit with the experimental one for $\Delta t = 6$ nm and $\Delta f = -65$ nm. It is worth mentioning that the domains are quite narrow, not exceeding approx. 2−3 nm along one direction. The small size of the domains is responsible for the broad reflections observed in the XRD pattern. In addition, the HREM image shows that the twins are coherent since no relative displacement is observed at the twin boundaries. This is outlined in Figure 5 and illustrated in the inset, where a schematic model of two domains of the ($\alpha = 3$ $\beta = 1$) structure meet at the (0001) twin plane. It can be appreciated that both domains are rotated 180° to one another around the twin plane.

The optical Fourier transforms corresponding to domains A and B (Figure 4a) are depicted in Figure 4c and Figure 4d, respectively. In domain A, the superstructure direction follows the $[44\bar{8}6]^*_{2H}$ reciprocal direction, while in domain B, tilted 90° with regard to the former, the satellite reflections are located along the $[\bar{4}\bar{4}86]^*_{2H}$ direction. In both domains, the intensity distribution of the spots is as expected for a modulated superstructure. The juxtaposition of both patterns (Figure 4e) corresponds to the experimental SAED shown in Figure 3a.

In the [0001]* reciprocal plane (Figure 6a) the reflections are distributed in a hexagonal array corresponding to a lattice parameter close to 0.9 nm. All the reflections are visible according to the trigonal *P*321 space group. The corresponding HREM (Figure 6b) also shows the presence of domains tilted by 60°, which are related to the previous twinning. Actually, in this image domains at 60° can be seen around the twin plane ($11\bar{2}0$); this is probably due to a mismatch between the chains.

$Ba_5Mn_3ZnO_{12}$

The SAED study of the title sample shows that it is not a single phase. It is worth noting that, in these 1D-phases, the most intense diffraction maxima are those corresponding to the 2H-subcell and, thus, they appear at very close d-spacings. This fact makes it difficult to detect small amounts of other members of the series that might be present as impurity phases in very small proportion by XRD. However, the SAED study reveals that, although almost all crystals correspond to the expected ($\alpha = 3$ $\beta = 2$) member of this series, a small fraction, presenting the structural features of the ($\alpha = 3$ $\beta = 3$) member, is also detected; such a

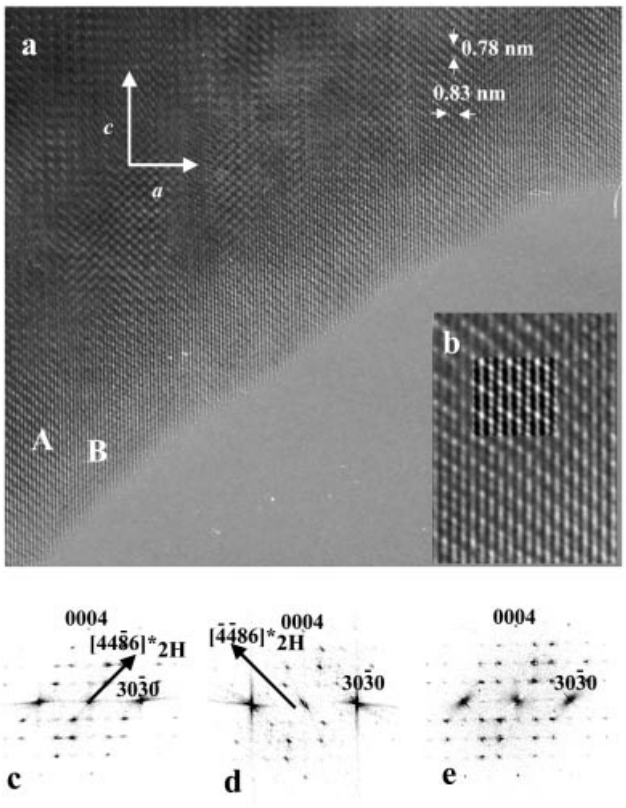

Figure 4. (a) HREM of $Sr_4Mn_2ZnO_9$ along [1$\bar{2}$10]; a twinned microstructure is clearly seen; (b) magnification of one of the microdomains shown in Figure 4a; the calculated image is shown in the inset; optical Fourier transforms (FT) corresponding to domains marked with A (c) and B (d) in Figure 4a; (e) FT corresponding to the juxtaposition of both A and B domains

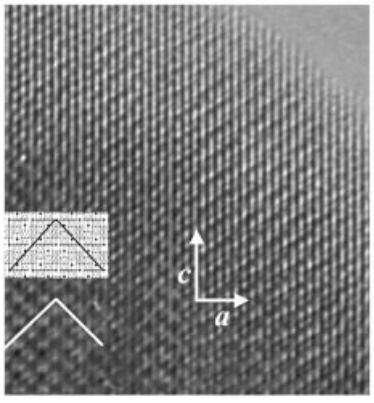

Figure 5. A magnification of the HREM image along [1$\bar{2}$10] showing a coherent twin structure; the twin boundary is labelled; a schematic model illustrating the twin boundary between two (α = 3 β = 1) domains is shown in the inset

member corresponds to the previously reported $Ba_6Mn_4ZnO_{15}$.[12] In spite of this, the majority of the phase corresponds to the new (α = 3 β = 2) member of the series and, therefore, we have performed the microstructural study of this phase.

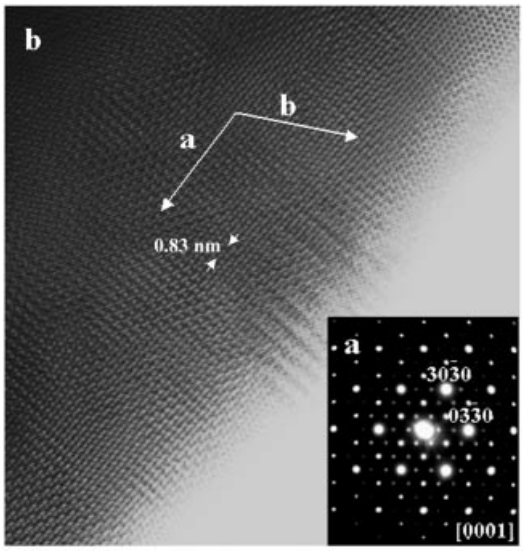

Figure 6. (a) SAED pattern corresponding to $Sr_4Mn_2ZnO_9$ along [0001]; (b) corresponding HREM image

The SAED pattern along the [1$\bar{2}$10] zone axis of the majority phase is shown in Figure 7a. EDS analysis performed on these crystals is in agreement with the nominal cationic ratio. The structural features of this pattern are those corresponding to the (α = 3 β = 2) member. Actually, only the 00l, $l = 2n$ reflections are visible ($P\bar{3}c1$ space group) and the modulation direction follows the $[55i6]^*_{2H}$ reciprocal axis. Once again, the intensity distribution of the spots suggests a twinned microstructure. As can be seen, satellite reflections appear not only along the $[55i6]^*_{2H}$ direction, as expected for this structure, but also along $[\bar{5}\bar{5}i6]^*_{2H}$ in a similar manner to that observed for $Sr_4Mn_2ZnO_9$. The presence of domains, tilted nearly 90° to each other, is clearly visible in the HREM taken along the [1$\bar{2}$10] direction (Figure 7b). Each domain shows the characteristic image of this (α = 3 β = 2) member and the calculated image (inset) is in agreement with the experimental one for Δt = 3.5 nm and Δf = −70 nm. The twin plane follows the [0001] direction, as in the previous case, but the domain size is much larger.

Taken together the SAED and HREM results indicate that both 1D oxides present a twinned microstructure. In order to establish if such a feature is a general characteristic of all Zn−Mn 1D oxides, we also studied oxide $Ba_6Mn_4ZnO_{15}$,[12] i.e., the (α = 3 β = 3) member of the series, by means of SAED and HREM. This oxide incorporates one more octahedron between the trigonal prisms than the previous $Ba_5Mn_3ZnO_{12}$ phase. The unit cell has rhombohedral symmetry ($R32$) with parameters a = 1.004 and c = 1.283 nm. The corresponding SAED pattern along [1$\bar{2}$10] is shown in Figure 8a. The superstructure spots appear not only along the $[66i6]_{2H}$ direction but also along the $[\bar{6}\bar{6}i6]_{2H}$ reciprocal direction and, consequently, a pseudotrigonal symmetry results. Once again, this is related to the presence of twinning as evidenced in the HREM along the

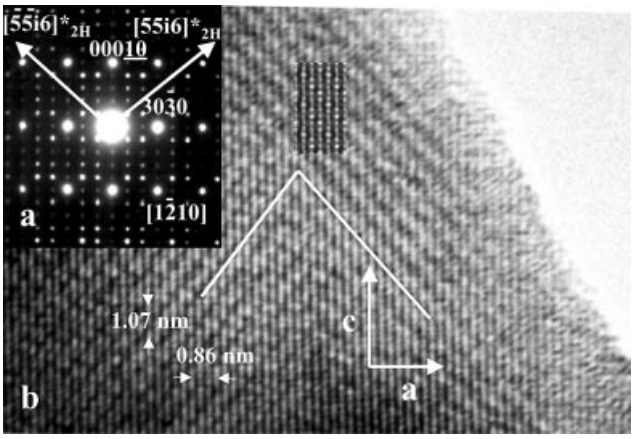

Figure 7. (a) SAED pattern corresponding to $Ba_5Mn_3ZnO_{12}$ along [1$\bar{2}$10]; (b) corresponding HREM image

same zone (Figure 8b). All the crystals checked exhibit the same features.

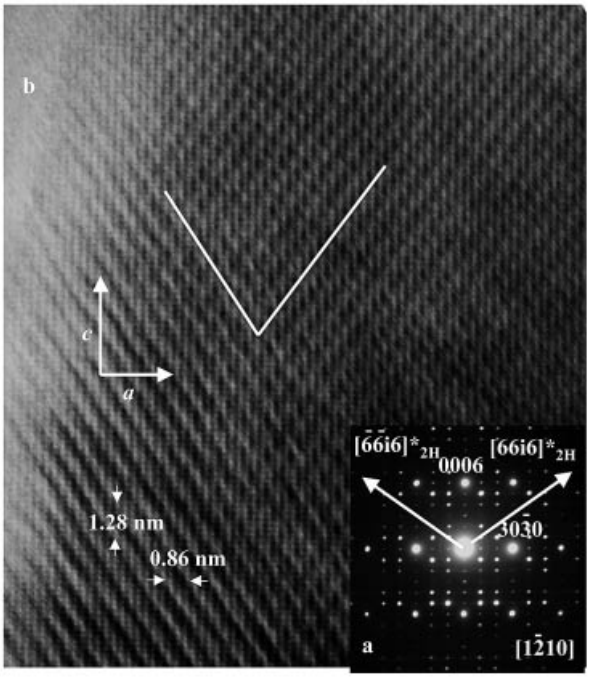

Figure 8. (a) SAED pattern corresponding to $Ba_6Mn_4ZnO_{15}$ along the [1$\bar{2}$10] zone axis; (b) corresponding HREM image; a twin plane is outlined

The stabilisation of one-dimensional oxides in the A−Mn−O system is a new example of the flexibility of the oxygen polyhedra chain in accommodating metal cations of very different size. The small size of Mn^{4+} (r_i = 0.53 Å) when compared with Zn^{2+} (r_i = 0.74 Å)[17] should give rise to a regular distribution of both transition metals in such a way that Zn would occupy the TP sites while Mn would be located in the octahedral ones. This is the case for Ca_3ZnMnO_6,[9] where [MnO_6] octahedra and [ZnO_6] trigonal prisms form a 1D chain with no sign of disorder between the metals over the two different sites. However, when the number of octahedra between trigonal prisms increases, it seems that both transition metals can be accommodated in the same oxygen environment. Neutron diffraction data on $Ba_6Mn_4ZnO_{15}$ [12] indicate that Mn^{4+} and Zn^{2+} ions are distributed in equal concentration in the trigonal prismatic polyhedra; consequently, Zn must also located in the octahedral sites.

The origin of the twinning cannot be easily determined, although it could be related to the cationic disorder in the structure. In this sense, it is worth noting that the presence of twinning related to cationic disorder has been previously reported in Sr_3CuPtO_6.[18] This compound crystallises in a distorted monoclinic structure (*C*2/*c*) closely related to the trigonal unit cell corresponding to the (α = 3 β = 0) member of this 1D homologous series. In this oxide, in which the single crystal X-ray diffraction data indicate that some disorder between Cu and Pt cations could exist, all crystals appear heavily twinned. Moreover, it is also noticeable that Ca_3ZnMnO_6,[9] in which an ordered distribution of Zn (into the TP sites) and Mn (into the O_h ones) is achieved, is the only 1D Zn/Mn-containing oxide that does not present a twinning microstructure. Figure 9 shows the SAED pattern corresponding to Ca_3ZnMnO_6 along the [1$\bar{2}$10] zone axis. A threefold superstructure is visible along the $[33i6]_{2H}$ reciprocal direction, corresponding to the (α = 3 β = 0) member of the series. The lack of superstructure maxima along the $[\bar{3}\bar{3}i6]_{2H}$ direction indicates that this is an untwinned compound. Although we do not have direct evidence of the cationic distribution in the new reported phases, it seems plausible to assume that increasing the number of octahedra between the trigonal prisms could facilitate the interchange between cations, giving rise to some cationic disorder. Such a disorder could be accompanied by local structural deformations which introduce some structural strain that is compensated by twin formation, as observed by HREM. The structural foundation of this observation will be further studied by neutron diffraction.

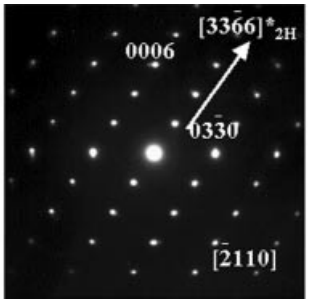

Figure 9. SAED pattern corresponding to Ca_3MnZnO_6 along [1$\bar{2}$10].

On the other hand, when the micrographs corresponding to $Ba_6Mn_4ZnO_{15}$ (Figure 8b), $Ba_5Mn_3ZnO_{12}$ (Figure 7b) and $Sr_4Mn_2ZnO_9$ (Figure 4a) are compared, it can be appreciated that the domain size decreases as the TP/O_h ratio increases. Actually, the highest concentration of twin planes is attained when the number of polyhedra per row and unit cell is lower. This feature seems to indicate that the struc-

tural strains are more pronounced when the Zn^{2+} ions can be distributed over a smaller number of octahedral sites. In addition, the smaller size of Sr^{2+}, in comparison to the Ba^{2+} cations, generates polyhedral sites of smaller volume, which increase the structural strain originating from the incorporation of Zn into the octahedral holes, thus supporting the small domain size in $Sr_4Mn_2ZnO_9$.

Magnetic Properties

The temperature dependence of the magnetic susceptibility corresponding to the single phase $Sr_4Mn_2ZnO_9$ measured at $H = 1000$ Oe is depicted in Figure 10a. The ZFC and FC data overlap in the temperature range measured and show a broad maximum at a temperature close to 100 K. At lower temperature (below 40 K), a sharp increase of the susceptibility is observed. The susceptibility curve cannot be fitted by a Curie−Weiss law over any temperature range.

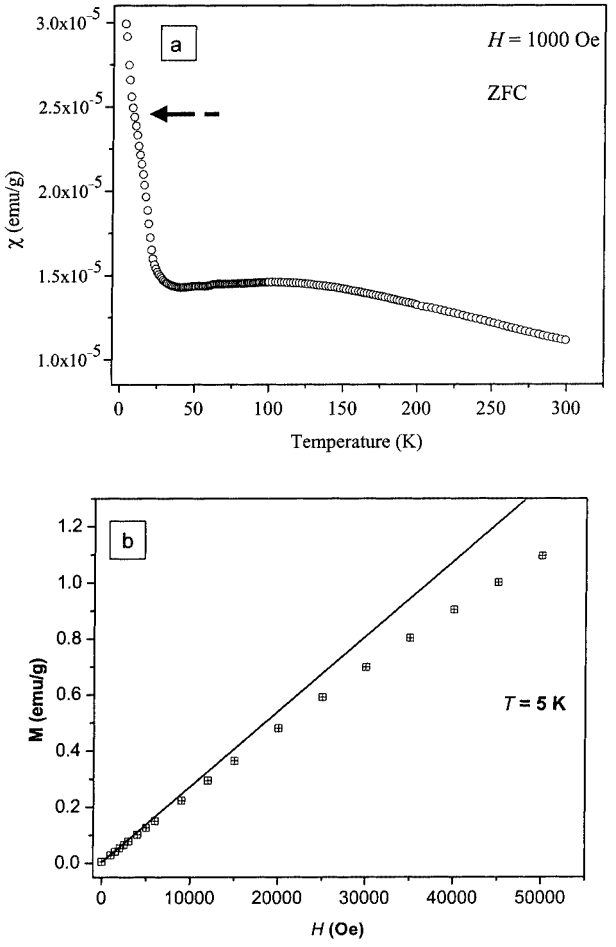

Figure 10. (a) Temperature dependence of the magnetic susceptibility of $Sr_4Mn_2ZnO_9$ at H = 1000 Oe; (b) magnetisation vs. applied field at 5 K; a nonlinear magnetisation field dependence is clearly observed

The magnetic behaviour of this 1D oxide is quite similar to that observed in $Ba_6Mn_4ZnO_{15}$,[12] although, in this case, the broad maximum is shifted to lower temperatures (50 K). The presence of such a maximum is characteristic of a 1D magnetic behaviour and it represents the onset of the 1D ordering along the chains. Such an ordering corresponds to antiferromagnetic interactions between Mn^{4+} in the chain, and therefore low magnetic susceptibility values are obtained in the measured temperature range. The increase of the number of octahedra between prisms seems to result in a weakening of the intrachain interactions and, consequently, the broad maximum is shifted to lower temperatures.

On the other hand, as can be observed in Figure 10a, the susceptibility passes through a local minimum and increases below 40 K. This rise of the magnetic susceptibility has also been observed in $Ba_6Mn_4ZnO_{15}$ and is associated with the presence of uncompensated magnetic moments that result from the irregular distribution of Mn^{4+} and Zn^{2+} in the polyhedra chains. Thus, these results agree with the presence of cationic disorder in the polyhedra chains in this new phase.

Unlike $Ba_6Mn_4ZnO_{15}$,[12] in which the 3D ordering is not observed in the magnetic susceptibility, the susceptibility curve corresponding to $Sr_4Mn_2ZnO_9$ shows a very small inflexion (marked in Figure 10a with an arrow) at about 7 K. This feature can be associated with a transition from 1D to 3D magnetic ordering. This weak interchain interaction is confirmed by slight nonlinear magnetisation-field dependence (Figure 10b). This different behaviour could be a consequence of the smaller interchain distance in the Sr compound due to their smaller size compared to Ba oxides.

It is worth recalling that a similar 1D-3D transition has previously been reported in Ca_3MnNiO_6.[9] The temperature-dependence susceptibility curve for this oxide is analogous to that corresponding to $Sr_4Mn_2ZnO_9$. Actually, a broad peak at around 100 K, attributed to a 1D antiferromagnetic ordering, and a small inflexion at 20 K, associated with a 3D ordering, are observed. This long range (3D) ordering has been confirmed by a neutron diffraction study.

Experimental Section

Polycrystalline $Sr_4Mn_2ZnO_9$ and $Ba_5Mn_3ZnO_{12}$ were synthesised by the ceramic procedure by heating stoichiometric amounts of ACO_3 (A = Sr, Ba; Aldrich, 99.9+%), $MnCO_3$ (Aldrich, 99.9+%) and ZnO (Aldrich, 99.99%) in air. The former was treated at 875 °C for five days and the latter at 1050 °C for six days with intermediate grindings. In both cases the products were quenched to room temperature.

The average cationic composition was determined by ICP while the local composition in every crystal was established by X-ray Energy Dispersive Spectroscopy (EDS). For this purpose, a JEOL 2000 FX electron microscope equipped with a OXFORD ISIS 300-analyser system was employed. Chemical compositions are consistent with the nominal ones.

Powder X-ray diffraction (XRD) patterns were collected with Cu-K_α radiation at room temperature on a PHILIPS X′PERT diffractometer equipped with a graphite monochromator.

Selected-area electron diffraction (SAED) was carried out using a JEOL 2000FX electron microscope fitted with a double-tilting

goniometer stage (±45°). High resolution electron microscopy (HREM) was performed on a JEOL 4000EX electron microscope fitted with a double-tilting goniometer stage (±25°). Simulated HREM images were calculated by the multislice method using the MacTempas software package.

Magnetic susceptibility was measured with a SQUID magnetometer in a temperature range from 5 to 300 K, under a maximum applied magnetic field of 5 T.

Acknowledgments

Financial support through research project MAT2001-1440 (CICYT, Spain) is acknowledged.

[1] J. J. Lander, *Acta Crystallogr.* **1951**, *4*, 148−156.
[2] G. Bergerhoff, O. Schmitz-Dumont, *Z. Anorg. Allg. Chem.* **1956**, *284*, 10−14.
[3] J. Darriet, M. A. Subramanian, *J. Mater. Chem.* **1995**, *6*, 543−552.
[4] P. D. Battle, G. R. Blake, J. Darriet, J. G. Gore, F. Weill, *J. Mater. Chem.* **1997**, *7*, 1559−1564.
[5] M. Evain, F. Boucher, O. Gourdon, V. Petricok, M. Dusek, P. Bezdicka, *Chem. Mater.* **1998**, *10*, 3068−3076.
[6] M. Zakhour-Nakhl, J. B. Claridge, J. Darriet, F. Weill, H. C. zur Loye, J. Pérez-Mato, *J. Am. Chem.* Soc. **2000**, *122*, 1618−1623.
[7] K. Boulahya, M. Parras, J. M. González-Calbet, *Chem. Mater.* **2000**, *12*, 25−32.
[8] S. Aasland, H. Fjellvåg, B. C. Hauback, *Solid State Commun.* **1997**, *3*, 187−192.
[9] S. Kawasaki, M. Takano, T. Inami, *J. Solid State Chem.* **1999**, *145*, 302−308.
[10] S. Niitaka, H. Kageyama, M. Kato, K. Yoshimura, K. Kosuge, *J. Solid State Chem.* **1999**, *146*, 137−143.
[11] J. Darriet, F. Grasset, P. D. Battle, *Mater. Res. Bull.* **1997**, *32*, 139−150.
[12] E. J. Cussen, J. F. Vente, P. D. Battle, *J. Am. Chem. Soc.* **1999**, *121*, 3958−3967.
[13] W. T. A. Harrison, S. L. Hegwood, A. J. Jacobson, *J. Chem. Soc., Chem. Commun.* **1995**, 1953−1954.
[14] K. Boulahya, M. Parras, J. M. González-Calbet, *J. Solid State Chem.* **1999**, *145*, 116−127.
[15] P. D. Battle, G. Blake, J. Sloan, J. F. Vente, *J. Solid State Chem.* **1998**, *136*, 103−114.
[16] K. Boulahya, M. Parras, J. M. González-Calbet, *J. Solid State Chem.* **1999**, *142*, 419−427.
[17] R. D. Shannon, *Acta Crystallogr., Sect. A* **1976**, *32*, 751−767.
[18] J. L. Hodeau, H. Y. Tu, P. Bordet, T. Fournier, P. Strobel, M. Marezio, *Acta Crystallogr., Sect. B* **1992**, *48*, 1−11.

Received April 21, 2002
[I02210]